ed that the population of this particular level corresponds to the destruction of the metastable $He(2^1S)$ atom.[5] Thus, we suggest that the destruction of metastable $He(2^3S)$ atoms in superfluid helium results in the population of high vibrational levels of the corresponding $a^3\Sigma_u^+$ molecular state. It is clear that further investigation of this phenomenon is necessary.

In summary, (a) the concentration of $He_2(a^3\Sigma_u^+)$ molecules in electron-bombarded superfluid helium is limited by collisions between pairs of these molecules. This bimolecular reaction is limited by $He_2(a^3\Sigma_u^+)$-roton collisions and the reaction coefficient is estimated to be about 2×10^{-10} cm^3/sec at a temperature of 2.08°K.[8] (b) The radiative lifetime of the $He_2(a^3\Sigma_u^+)$ state in superfluid helium exceeds 0.1 sec. (c) Approximately 500 $He_2(a^3\Sigma_u^+)$ molecules are produced in the superfluid per incident 160-keV electron. (d) The lifetime of the $He(2^3S)$ state in the superfluid is about 15 μsec and approximately 450 $He(2^3S)$ atoms are produced per incident 160 keV electron. (e) We suggest the destruction of $He(2^3S)$ atoms in superfluid helium results in the population of high vibrational levels of the corresponding $He_2(a^3\Sigma_u^+)$ molecular state.

*Work supported in part by the National Science Foundation.

[1]C. M. Surko and F. Reif, Phys. Rev. 175, 229 (1968).
[2]W. S. Dennis, E. Durbin, Jr., W. A. Fitzsimmons, O. Heybey, and G. K. Walters, Phys. Rev. Lett. 23, 1083 (1969).
[3]J. C. Hill, O. Heybey, and G. K. Walters, Phys. Rev. Lett. 26, 1213 (1971).
[4]M. Stockton, J. W. Keto, and W. A. Fitzsimmons, Phys. Rev. Lett. 24, 654 (1970). See also C. M. Surko, R. E. Packard, G. J. Dicke, and F. Reif, Phys. Rev. Lett. 24, 657 (1970).
[5]M. Stockton, J. W. Keto, and W. A. Fitzsimmons, Phys. Rev. A 5, 372 (1972).
[6]A. P. Hickman and N. F. Lane, Phys. Rev. Lett. 26, 1216 (1971).
[7]J. Wilks, *Liquid and Solid Helium* (Clarendon, Oxford, England, 1967), p. 119.
[8]Our values for the concentrations of metastable states agree well with those of Ref. 3, and our results for $\alpha(T)$ are in good agreement with the single measurement at 1.7°K of J. C. Hill, O. Heybey, and G. K. Walters, Phys. Rev. Lett. 26, 1519(E) (1971).
[9]A lower limit of about 0.05 sec for the radiative lifetime of the metastable helium molecule in helium gas at 300°K has been established previously. See A. V. Phelps, Phys. Rev. 99, 1307 (1955). The three-body conversion of the $He(2^3S)$ atom into a $(v=0)$ $He_2(a^3\Sigma_u^+)$ molecule is also reported in this paper.
[10]Hill *et al.* (Ref. 3) report a lifetime of 1 msec for the $He(2^3S)$ state in superfluid helium.
[11]M. L. Ginter and R. Battino, J. Chem. Phys. 52, 4469 (1970).

Resonant Absorption of Laser Light by Plasma Targets*

J. P. Freidberg, R. W. Mitchell, R. L. Morse, and L. I. Rudsinski
University of California, Los Alamos Scientific Laboratory, Los Alamos, New Mexico 87544
(Received 28 October 1971)

It is proposed that a resonant mechanism should cause significant absorption of energy from intense laser pulses in plasma targets, and that the energy should be deposited in such a way as to form a very non-Maxwellian high-temperature tail on the electron velocity distribution.

Current interest in the controlled release of nuclear energy from laser-heated pellets of thermonuclear fuel has drawn interest to mechanisms by which laser light might be absorbed in the surface of such pellets. The large pulsed light intensities which are required for this heating and are beginning to be available in absorption experiments put the interaction of the laser radiation with the initially solid target in the approximately collisionless regime. Binary collisions between electrons driven by the wave fields and ions (sometimes called inverse bremsstrahlung) can cause some absorption and may be quite important in allowing a weak precursor of a pulse to ionize the target and give the surface some thickness as assumed below, but as the intensity increases, the fraction of the light energy absorbed by collisions becomes smaller.

In this Letter we propose a resonant, collisionless absorption mechanism by which an inhomogeneous target plasma can absorb a significant fraction of obliquely incident laser light. We then show from numerical simulations that the energy is deposited in a very non-Maxwellian tail

of the electron velocity distribution. Preliminary work on a relativistic absorption mechanism is also mentioned. If the electron density of the plasma n_e and therefore the dielectric constant ϵ are functions only of x (the light is incident with the wave vector $\vec{k}$ in the x,y plane at an angle θ to the x axis, and the field $\vec{E}$ is polarized in this plane), then the cw wave equation for the only nonzero component of the magnetic field, B_z, is

$$\frac{d^2B_z(x)}{dx^2} - \frac{1}{\epsilon(x)}\frac{d\epsilon}{dx}\frac{dB_z(x)}{dx} + k_0^2(\epsilon - \sin^2\theta)B_z(x) = 0, \quad (1)$$

where $k_0 = \omega_0/c$ is the free-space wave number and $B_z(x,y,t) = B_z(x)\exp(-i\omega_0 t + ik_y y)$, with $k_y = k_0 \times \sin\theta$. Consider the familiar dielectric constant for a cold plasma with a collision frequency ν:

$$\epsilon(x) \simeq 1 - \frac{\omega_{pe}^2(x)}{\omega_0^2}\left(1 + \frac{i\nu}{\omega_0}\right), \quad \frac{\nu}{\omega_0} \ll 1, \quad (2)$$

where $\omega_{pe} = (4\pi n_e e^2/m_e)^{1/2}$ is the electron plasma frequency. In the collisionless limit, $\nu/\omega_0 \to 0$, a resonant singularity appears in the second term in Eq. (1) at the point on the density profile where $\omega_{pe}(x) = \omega_0$ and, therefore, $\epsilon(x) \to 0$. (By contrast no such resonant singularity appears in the corresponding equation for light polarized normal to the plane of incidence.) In this limit a finite absorption occurs at the singularity. When Eq. (1) is integrated with a linear density gradient such that the density rises linearly from $\omega_{pe} = 0$ at $x = 0$ to $\omega_{pe} = \omega_0$ at $x = L$, and the connection formulas at the singularity are given only by $\nu > 0$ and $\nu/\omega_0 \to 0$, the power absorption coefficients plotted in Fig. 1 are obtained. The maxima indicate that there is an optimum angle of incidence for absorption. For $k_0L = 10$ this is seen to be at

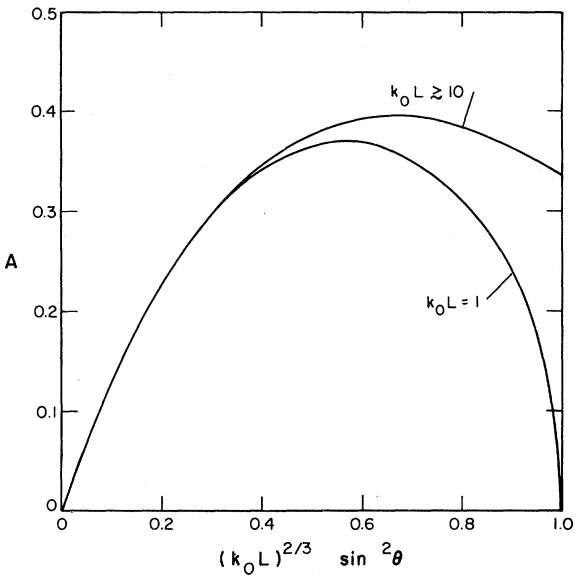

FIG. 1. Power absorption coefficient A as a function of angle of incidence θ, vacuum wave number k_0, and distance from the front edge to the critical surface, L.

$(k_0L)^{2/3}\sin^2\theta \simeq 0.7$ or $\theta \simeq 23°$. For large L, i.e., weaker density gradients, the optimum angle is smaller, i.e., more nearly normal incidence. Figure 2 shows real and imaginary parts of the nonzero components of the solution of Eq. (1) when $k_0L = 10$ and $\theta = 23°$. The phase of the wave, i.e., the choice of real and imaginary parts is taken to be such that B_z is pure real at $x = L$ [Fig. 2(a)]. The absorption is caused by the nonzero wave field E_x, which only occurs when there is non-normal incidence with this polarization, and which drives plasma oscillations in the x direction with frequency ω_0. At the critical surface where $\omega_0 = \omega_{pe}$, the natural frequency of these plasma oscillations, their amplitude becomes

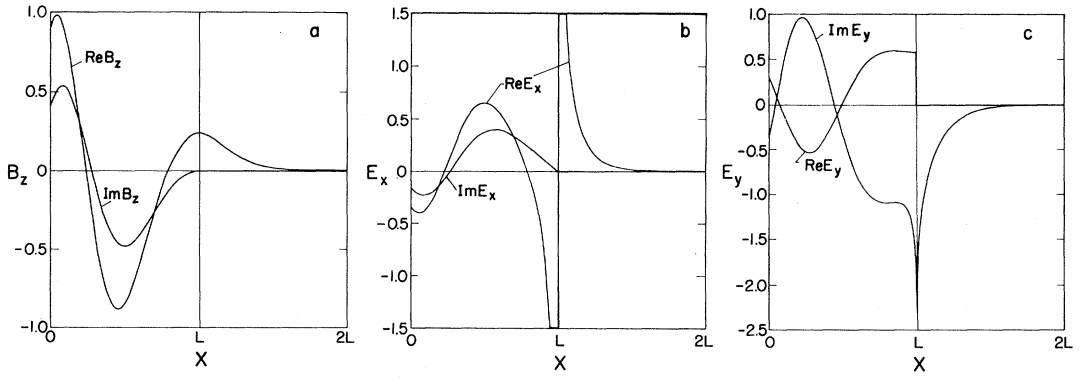

FIG. 2. The various nonzero electromagnetic field components from the case $k_0L = 10.0$ at the optimum angle of $\theta = 23°$ in the limit $\nu/\omega \to 0$.

very large, in fact inversely proportional to ν; and as $\nu \to 0$ the collisional energy dissipation smoothly approaches the finite limit plotted in Fig. 1. From Fig. 2 the x component of the Poynting vector is a step function, finite and constant to the left of $x = L$ and falling to zero there with $\mathrm{Re}E_y$ [Fig. 2(c)], where $\mathrm{Re}B_z$ [Fig. 2(a)] remains finite. This is consistent with a very large real x component of the electron current, J_x, at $x = L$ which is in phase with, and therefore absorbs energy from, the electromagnetic part of $\mathrm{Re}E_x$. {$\mathrm{Im}E_x$ is zero at $x = L$ [Fig. 2(b)], except for a δ function there, which does not appear explicitly in the calculations and does not contribute directly to the absorption in this approximation.} This part of E_x, which drives the oscillations in the first place and which is nonsingular at $x = L$, is reduced to zero by the changing x projection as $\hat{k}_0$ turns toward normal incidence and is reduced by the increased tunneling distance from the classical turning point where $\omega_{pe}^2/\omega_0^2 = \cos^2\theta$ to $x = L$ where $\omega_{pe}^2/\omega_0^2 = 1$ when θ becomes large. Hence there is a maximum absorption at intermediate values of θ, an argument which can be formalized to estimate that the maximum occurs where $(k_0 L)^{2/3}\sin^2\theta \simeq (\frac{1}{2})^{2/3}$.

The linear density profile is qualitatively like most of the profiles expected in practice when an initially sharp surface expands a bit into the vacuum during heating, sometimes because of a weak precursor before a short main pulse. Of course the magnitude of the absorption will depend somewhat on the details of the profile. For instance a more nearly flat spot in the profile near the critical surface can enhance the absorption.

Collisional resonant absorption of obliquely incident radiation has been studied previously by the model used above, but without numerical integrations, in the context of microwave propagation in the ionosphere.[1] Essentially the same effect seems to be observed in studies of the infrared irradiation of thin metal films.[2]

The preceding linearized treatment implicitly assumes that the amplitude of the x displacements of the electrons, which in steady state is

$$\xi(x) = \frac{eE_d}{m_e[\omega_0^2 - \omega_{pe}^2(x) - i\nu\omega_0]}, \qquad (3)$$

where E_d is the electromagnetic part of E_x referred to above which drives the oscillations, is so small that it can be neglected.

However, for any given amplitude of wave field there is some region around the critical surface where this is not true when $\nu/\omega_0 \to 0$ and where, in fact, the condition for phase-space breaking, $|d\xi/dx| > 1$, is satisfied. In this collisionless regime the breaking of the electron plasma waves, or oscillations, in the resonant region takes the place of collisions in damping the amplitude of the oscillations and thereby absorbing wave energy. Though we consider initially relatively cold electrons here, this breaking would go over to Landau damping when the electrons are initially sufficiently warm. In order to reach this understanding of the collisionless resonant absorption, which is quite nonlinear, it was necessary to treat the problem by particle-in-cell numerical simulation.[3] Since the problem is basically two-dimensional (except for a version of the problem which is infinite but *not* periodic in y), a self-consistent treatment required fully electromagnetic two-dimensional (in x and y) simulations which were done using the method of Appendix B in Ref. 3 with periodicity in y. The results of these two-dimensional simulations, which will be published in a more complete article, show that the following one-dimensional simulation method gives a qualitatively correct picture of the collisionless resonant electron heating in addition to affording higher spatial resolution. An oscillating field $E_d(x, t)$ is arbitrarily imposed, as in Eq. (3) above, with a smooth bell-shaped profile in x centered at $x = L$ and broad enough that the resulting electron distribution is insensitive to its width. The electrons, and the ions if they are mobile, move in x and their resulting charge density is used to compute an additional electrostatic field E_x from Poisson's equation as if the system were independent of y. This E_x added to E_d determines the motion of the particles. In the dimensionless units of the simulation Fig. 3, a particle with unit velocity travels a unit distance in a unit time; and the frequency of E_d, which is of course equal to the plasma frequency at the critical surface, is $\omega = 1$, i.e., a period of the driving field is 2π. The maximum amplitude of E_d at $x = L$ is such that a free electron would oscillate with a maximum x velocity V_d of 1, which is much less than the resonantly enhanced values seen in Fig. 3.

At $t = 0$ (Fig. 3) the electrons, which are cold, and the ions, which are fixed, have a linear density profile which rises from zero at $x = 0$ to twice the critical density at $x = 2L = 600$, with the critical density at $x = L = 300$. The sinusoidal oscillations of E_d begin at this time and the oscillations build up without breaking until at $t = 41$

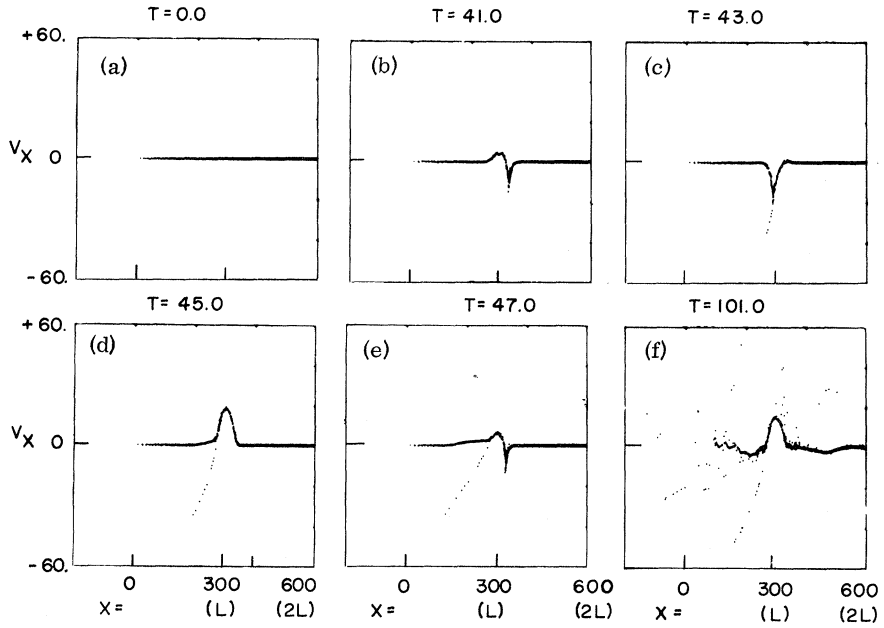

FIG. 3. Electron phase-space plot of a one-dimensional simulation of the collisionless absorption. Note the few scattered electrons at large energies in (d), (e), and (f).

through 43, breaking occurs for the first time. Equation (3) (with $0<\nu/\omega_0\ll 1$ near $x=L$ to represent the damping effect of breaking) shows that oscillations on either side of $x=L$ should be 180° out of phase with one another, with those very close to $x=L$ being 90° out of phase with both in such a sense that the total wave motion near $x=L$ appears like a sequence of waves growing up on the high-density side and moving toward the lower-density side followed by a rarefaction-like motion back to the high-density side as seen at $t=45$. Hence, as observed here, the breaking should occur to the left, i.e., toward the vacuum, and not to the right. At $t=47$, the high-energy electrons from the first breaking are moving toward the vacuum where they will be reflected back to the right by a charge separation potential (as seen later at $t=101$). The breaking process at the critical surface is about to repeat as it does on every cycle from then on in about the same way if, as in this code, the hot electrons are absorbed at the right wall and replaced by re-emission of cold electrons. The energy is then effectively deposited in the interior of the target by collisionless electron thermal conductivity, as seen at $t=101$. Plainly, the heated electrons are much more energetic than they would be with the maximum free-electron velocity of $V_x=V_d=1$ and thus constitute a very non-Maxwellian high-temperature tail on an otherwise essentially cold electron velocity distribution. Figure 4 shows the distribution of ions at $t=200$ from an otherwise identical run but with mobile H^+ ions. Electron pressure is causing the front-surface ions to blow off with a rather high energy and is pushing ions away from the critical surface, which has the effect of temporarily partially quenching the resonance.

The breaking condition $|d\xi/dx|=1$, applied to Eq. (3) with $\nu/\omega_0=0$, gives a maximum velocity for the heated electrons of $V_{max}=(\omega_0 V_d L)^{1/2}$ which in the units of Fig. 3 is $V_{max}\simeq 35$ and agrees with the simulations. When $\nu(x)/\omega_0$ is adjusted to nonzero values in the breaking region to hold ξ down to the breaking condition and thus simulate the damping effect of breaking, the absorption rates of Fig. 1 are seen to be approximately correct

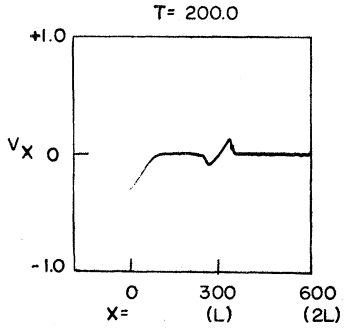

FIG. 4. Phase-space plot of H^+ ions.

for collisionless absorption and the mean energy of the heated electrons can be estimated to be

$$\langle \mathcal{E} \rangle = (m_e \omega_0 P_A / n_c')^{1/2},$$

where P_A is the absorbed power per unit surface area and n_c' is the electron density gradient at the critical surface.

Recent one- and two-dimensional simulations including relativistic particle dynamics have also shown that when the laser wave field is sufficiently intense that the cyclotron frequency $\omega_{ce} > \omega_{pe}$ for a significant distance on the overdense side of the critical surface, a significant fraction of the incident energy is imparted to the electrons in a manner similar to that seen above by the oscillating radiation pressure, i.e., the $\vec{V} \times \vec{B}$ force. Here, however, polarization and angle of incidence are not so important, and the resulting electron energy distribution shows less of the two-temperature structure seen above.

This work was first presented at the September 23–27, 1971 Gordon Conference on the Interaction of Laser Light with Matter.

*Work performed under the auspices of the U. S. Atomic Energy Commission.

[1]P. Hirsch and J. Shmoys, J. Res. Nat. Bur. Stand., Sect. D 69, 521 (1965), and references contained therein.

[2]M. Skibowski, B. Fenerbacher, W. Steinmann, and R. P. Godwin, Z. Phys. 211, 329 (1968).

[3]R. L. Morse and C. W. Nielson, Phys. Fluids 14, 830 (1971).

Sound Velocity in a Nematic Liquid Crystal*

M. E. Mullen, B. Lüthi, and M. J. Stephen

Department of Physics, Rutgers, The State University, New Brunswick, New Jersey 08903

(Received 15 February 1972)

We have made sound-velocity measurements in the liquid crystal *p*-methoxy-benzylidine, *p*-*n*-butyl-aniline. Near the nematic-isotropic phase transition we observe a dispersion in the sound velocity. Quantitative measurements are presented on the sound-velocity anisotropy in an oriented liquid crystal.

It was found recently that the attenuation of ultrasonic waves shows an angular dependence in nematic liquid crystals,[1-3] the attenuation being higher for the propagation direction along an applied magnetic field and smaller for propagation perpendicular to the field. In all these papers it was noted that the corresponding velocity anisotropy, if any, was very small, typically 0.1% and smaller. Therefore, phase-sensitive detection is necessary in order to make a quantitative study of this effect.

We would like to report here on the first such velocity measurements using the liquid crystal *p*-methoxy-benzylidine, *p*-*n*-butyl-aniline (MBBA).[4] Our apparatus for the measurement of sound velocity has been described elsewhere,[5] and is very well suited for conditions where the attenuation is high. The measurement consists of a phase comparison, where the phase change of a pulse-modulated echo is compared with the stable cw source. For our measurements the resolution was typically 3 parts in 10^6 for relative changes in velocity. The sample was placed in brass cylinders using several different lengths (2.5, 4.8, and 7.3 mm), and the temperature was varied and stabilized by a heater with feedback control. The temperature stability was better than 0.1°C.

We first show our experimental results and then attempt to interpret them. In Fig. 1 we

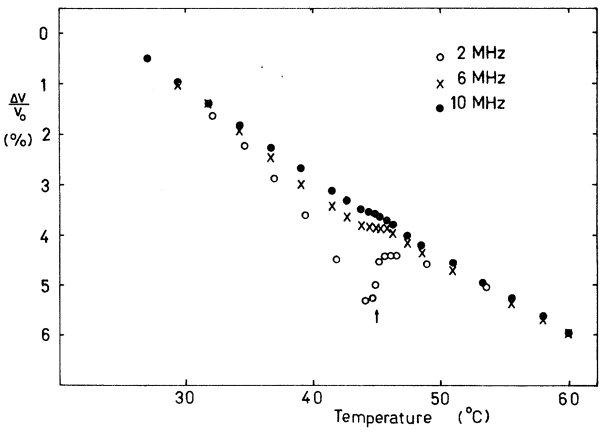

FIG. 1. Relative velocity changes for different frequencies as a function of temperature. Arrow indicates attenuation maxima at 45°C.